



# Numerical Investigation of the Effect of Ethylene Glycol with SnFe<sub>2</sub>O<sub>3</sub> Hybrid Nanofluid on Heat Transfer in Flat, Face Step, and Radial Corrugated Microchannels

Hashim Alsammarraie<sup>1</sup>, Mohd Khairol Anuar Mohd Ariffin<sup>1,\*</sup>, Eris Elianddy Supeni<sup>1</sup>, Siti Ujila Masuri<sup>1</sup>

<sup>1</sup> Mechanical and Manufacturing Engineering Department, Universiti Putra Malaysia, 43400 Seri Kembangan, Selangor, Malaysia

## ARTICLE INFO

### Article history:

Received 6 April 2023

Received in revised form 4 May 2023

Accepted 7 June 2023

Available online 1 October 2023

### Keywords:

Nanofluid; Hybrid Nanofluid; heat transfer; Microchannel; heat exchangers

## ABSTRACT

Nanofluid technology is one of the latest technics aims to enhance the heat exchangers working systems. The nanofluid is used because it has better thermal performance properties than common fluids like water. Tin Oxide (SnO<sub>2</sub>) and Ferric Oxide (Fe<sub>2</sub>O<sub>3</sub>) has used due to their availability and low cost for manufacturing. Flat, face step and radial corrugated microchannels have been studied at the Reynolds number range (4000-7000 Re). In this study, a hybrid nanofluid combined Ferric Oxide and Tin Oxide SnFe<sub>2</sub>O<sub>3</sub> at (0, 5, 15%) of Tin Oxide concentration. The volume concentration of the nanoparticles was from (1-5)% suspended in ethylene glycol as base fluid due to its high thermal performance compared with water. The performance evaluation criteria (PEC) are studied and the results were validated with experimental and numerical results from previous studies. Performance evaluation criteria (PEC) studied the heat transfer in all study steps and found that the <sup>15</sup>Sn<sup>85</sup>Fe<sub>2</sub>O<sub>3</sub> hybrid nanofluid in ethylene glycol at 5% volume concentration in radial corrugated microchannel increased 104% compared with base fluid ethylene glycol in the flat microchannel. The performance evaluation criteria value has increased by 82% from flat microchannel to radial microchannel at 5% of volume concentration of <sup>15</sup>Sn<sup>85</sup>Fe<sub>2</sub>O<sub>3</sub> hybrid nanofluid.

## 1. Introduction

In recent years, heat transfer enhancement and optimization have received much attention to improving the heat exchanger design with high thermal efficiency models by using novel methods to reduce the operational cost and energy consumption which is important in the industrial area. The researchers developed the heat exchangers by suspending high thermal efficiency nanoparticles in the base fluid which is inside the heat exchanger channels to improve the effective thermal efficiency of the working fluid and to increase the differences in the temperature between the surface and fluid.

\* Corresponding author.

E-mail address: [khairol@upm.edu.my](mailto:khairol@upm.edu.my) (Mohd Khairol Anuar Mohd Ariffin)

<https://doi.org/10.37934/cfdl.15.10.7192>

Those factors have been studied numerically, experimentally, and theoretically, by Akbari *et al.*, [1], Dogonchi *et al.*, [2], Thumma *et al.*, [3], and Eshgarf *et al.*, [4]. Those studies found that the additional nanoparticles increased the thermal efficiency of the heat exchanger systems.

This modern class of fluids consists of pendant nanoparticles with high suspension stability compared to the micrometer and millimeter-sized particles. Lately, studies focused on the base fluid that the nanoparticles will be suspended in have been improved by mixing the water and the ethylene glycol or glycerine because those fluids were found to improve the thermal efficiency of the nanofluid and the whole system [5].

In the last few decades, researchers used many different designs for the heat exchanger channels to increase thermal efficiency and improve the system by using corrugated channels to increase the thermal contacted surface area and the thermal resistance in a single spot. In the past few years, the demand for microchannel heat exchangers had increased in many industrial applications. There are three types of heat transfer enhancement techniques: active methods, passive methods, and compound methods mixed between active and passive.

Recently nanofluid in its two types metallic and non-metallic take huge attention for what it has achieved in this field. Many researchers cited that about 15-48% of heat transfer efficiency can be achieved by using nanofluid instead of traditional fluids such as pure water [6]. With these magnificent changes, the weight and the size of the heat exchanger can be reduced without affecting the heat transfer performance, which leads to reduced energy consumption, manufacturing cost, and operational costs from the system.

Nanofluid is liquid content of metallic, non-metallic, or hybrid nanoparticles with a 0.1-100nm size suspended in a base fluid, such as (water, ethylene glycol, glycerine, acetone, etc.) [7-10]. In recent years, it has been noticed that the addition of nano-sized particles to the base fluid can improve its thermal conductivity in multi industrial applications [11,12]. This research presents the latest enhancement in each character that can change the thermal conductivity and the heat transfer quantity, this research aims to aggregate the latest research on the nanofluid technology to simplify to the researchers about the latest trends and the recommendations for new researchers based on authors' knowledge. Many researchers applied this magnificent fluid in many heat exchanger applications that will enhance the heat transfer coefficient which increases the heat exchanger efficiency [13]. Several review papers have been published concerning the synthesis and applications of the usage of nanofluids such as Chiam *et al.*, [6], Kleinstreuer and Feng [14], Das *et al.*, [15], Yu *et al.*, [16], Salman *et al.*, [17], and Urmi *et al.*, [18]. The nanofluid is regarded as a novel class technique to optimize the heat transfer efficiency of the heat exchangers owing to the high dispensability of the nanoparticles within the base fluid and the high stability of the suspension. Ajith *et al.*, [19] studied the enhancement in thermal conductivity of mixing  $MgFe_2O_4$  hybrid nanoparticles with water as base fluid to prepare hybrid nanofluid with high thermal conductivity in different volume fractions as shown in Figure 1. Figure 2 shows the Nusselt number increasing in different Reynolds numbers (3000, 4500, 6000, 7500 Re) for different volume fractions of CuO/Water nanofluid of a conducted study by Bazdar *et al.*, [20]. Heat transfer enhancement using hybrid  $MnFe_2O_4$  – ethylene glycol has been studied experimentally in a mini shell and tube heat exchanger by Firlianda *et al.*, [21] has been successfully carried out, the researchers studied the effect of adding  $MnFe_2O_4$  to ethylene glycol as base fluid, the results of heat transfer analyzed by using LMTD method, the highest value was obtained at 0.075% of nanoparticles concentration of  $MnFe_2O_4$ .

A review of previous studies presented that the existing papers have not studied the hybrid  $SnFe_2O_3$ , and the ethylene glycol as base fluid with the hybrid nanoparticles and have not investigated that in flat or face step or radial corrugated microchannels, which is the aim of this research.

## 2. Problem Description and Boundary Conditions

Figure 1 shows the basic geometry of the channels investigated in this study, flat, face step, and radial corrugated microchannels. For the flat microchannel, the geometry will be smooth, the hydraulic diameter was  $900\mu\text{m}$ , and the channel length was  $30\text{mm}$ . Two adiabatic smooth sections are used as the boundary conditions for both inlet and outlet of the channels, one upstream section (developing section) and the other downstream section (exit section).

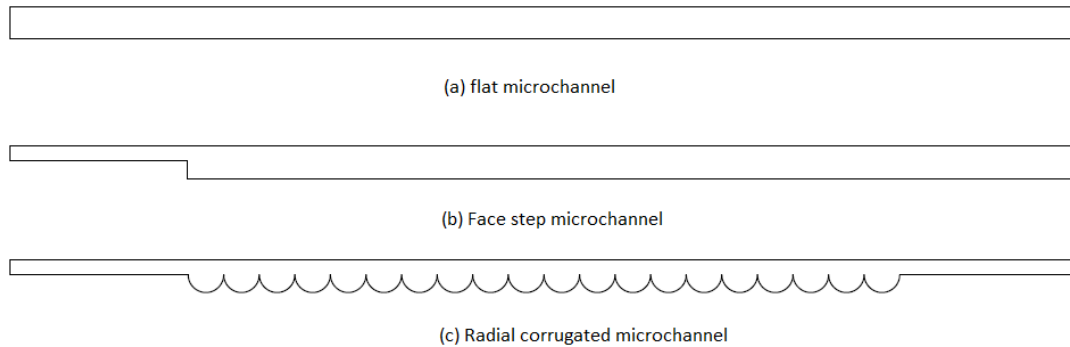


**Fig. 1.** (a) Flat, (b) face step and (c) radial corrugated microchannel

The flow was assumed to be steady, incompressible, and three-dimensional. Assuming water and ethylene glycol as base fluids and hybrid tin oxide doped in ferric oxide are solid spherical shape Nano-sized particles were in thermal equilibrium. Lastly, assuming the nanofluids are Newtonian fluids.

To solve the governing equations, firstly, must define appropriate boundary conditions for all dependent variables on all the boundaries of the domains. The Reynolds numbers were 4000, 5000, 6000, and 7000. The velocity was fully developed, and uniform temperature distributions are commonly assumed in the inlet of the channel. For the inlet section suitable correlations have been used to calculate the inlet velocity. The proper position of the outlet boundary is the region where equilibrium takes place in the direction of the flow. This corresponds to the fully developed regions. For the top and bottom walls of the channel wall, a no-slip boundary condition can be applied for the velocities. Uniform heat flux ( $250\text{ W/m}^2$ ) conditions are applied along the walls channel. The working fluids were distilled water, ethylene glycol,  $\text{Fe}_2\text{O}_3$ ,  $^{55}\text{Sn}^{95}\text{Fe}_2\text{O}_3$ , and  $^{15}\text{Sn}^{85}\text{Fe}_2\text{O}_3$  at 1-2-3-4-5 % of volume concentration in ethylene glycol as base fluid.

The boundary conditions used at the solid walls are fundamentally no-slip boundary conditions concerning the wall temperature. Ambient conditions (*i.e.*, ambient pressure and temperature) are used for the inlet whereas uniform ambient pressure condition is used at the outlet.

## 3. Governing Equations

In this model, it is possible to assume that the mixture is in a homogeneous state when the nanoparticles are mixed with base fluid and they flow at the same velocity. So, it is assumed that the nanofluids are a homogenous mixture. However, the governing equations and the turbulent modeling can be written as [22]:

Continuity equation:

$$\nabla \cdot (\rho_{nf} v) \quad (1)$$

Momentum equation:

$$\frac{\partial(\rho u_i u_j)}{\partial x_j} = -\frac{\partial p}{\partial x_i} + \frac{\partial}{\partial x_j} \left[ \mu \left( \frac{\partial u_i}{\partial x_j} + \frac{\partial u_j}{\partial x_i} \right) \right] - \frac{2}{3} \mu \frac{\partial u_k}{\partial x_k} \delta_{ij} \quad (2)$$

Energy equation:

$$\frac{\partial}{\partial x_j} \left( \rho u_j C_p T - k \frac{\partial T}{\partial x_j} \right) = u_j \frac{\partial p}{\partial x_j} + \left[ \mu \left( \frac{\partial u_i}{\partial x_j} + \frac{\partial u_j}{\partial x_i} \right) - \frac{2}{3} \mu \frac{\partial u_k}{\partial x_k} \delta_{ij} \right] \quad (3)$$

In the current study, the k-ε RNG turbulence model is employed as follows:

$$\frac{\partial}{\partial x_i} (\rho k u_i) = \frac{\partial}{\partial x_j} \left[ \left( \mu + \frac{u_t}{\sigma_k} \right) \frac{\partial k}{\partial x_j} \right] + G_k - \rho \varepsilon \quad (4)$$

Likewise, the dissipation rate of TKE is assumed by the equation:

$$\frac{\partial}{\partial x_i} (\rho \varepsilon u_i) = \frac{\partial}{\partial x_j} \left[ \left( \mu + \frac{u_t}{\sigma_k} \right) \frac{\partial \varepsilon}{\partial x_j} \right] + C_{1\varepsilon} \frac{\varepsilon}{k} G_k - C_{2\varepsilon} \rho \frac{\varepsilon^2}{k} \quad (5)$$

Where  $G_k$  is the rate of generation of the TKE while  $\rho$  is the destruction rate is written as:

$$G_k = \left( -\overline{\rho u_i u_j} \right) \frac{\partial u_j}{\partial x_i} \quad (6)$$

### 3.1 Thermophysical Properties of Nanofluids

First, the thermophysical properties of the nanofluids were calculated to be used in the simulation program to modify the state of the nanofluid combination. Different types of nanoparticles were tested  $\text{Fe}_2\text{O}_3$ , hybrid  $^{55}\text{Sn}^{95}\text{Fe}_2\text{O}_3$ , and  $^{15}\text{Sn}^{85}\text{Fe}_2\text{O}_3$ . The thermophysical properties for simulations are thermal conductivity ( $k_{nf}$ ), mass density ( $\rho_{nf}$ ), dynamic viscosity ( $\mu_{nf}$ ), and specific heat ( $c_{p,nf}$ ). Considering these are the properties of thermal conductivity, mass density, viscosity, and specific heat are calculated according to the mixing theory.

#### 3.1.1 Thermal conductivity

The Maxwell model equation has been used to calculate the nanofluid thermal conductivity. Manay and Sahin [23] studied experimentally the thermal conductivity of a ferrite nanofluid and then compared the results with many studies and that resulted that the Maxwell model gave closer predictions to the experimental results.

$$k_{nf} = k_{bf} \left[ \frac{k_p + 2k_{bf} + 2(k_p - k_{bf})\phi}{k_p + 2k_{bf} - (k_p - k_{bf})\phi} \right] \quad (7)$$

Where  $k_{nf}$  is the nanofluid thermal conductivity,  $k_{bf}$  is the base fluid thermal conductivity,  $k_p$  refers to the particle's thermal conductivity, and  $\phi$  is the nanoparticles volume fraction.

### 3.1.2 Density

Eq. (3) calculating the density of the nanofluid was applied in many studies and got a high accuracy [21,24].

$$\rho_{nf} = (1 - \phi)\rho_{bf} + \phi\rho_p \quad (8)$$

$\rho_{nf}$  refers to the density of the nanofluid,  $\rho_p$  means the density of nanoparticles,  $\rho_{bf}$  is the density of the base fluid and  $\phi$  is the volume fraction of the nanofluid.

### 3.1.3 Specific heat

The specific heat of the nanofluids has been calculated based on the Xuan and Rotzel's [25] equation at constant pressure:

$$Cp_{nf} = (1 - \phi)Cp_{bf} + \phi Cp_p \quad (9)$$

$Cp_{nf}$  refers to the specific heat amount of the nanofluid,  $Cp_{bf}$  means the heat capacity of the base fluid,  $Cp_p$  is the specific heat of the nanoparticles and  $\phi$  is the volume fraction of the nanofluid.

### 3.1.4 Viscosity

The last measurement of thermophysical properties is viscosity, which expresses the viscosity value of the fluid, and the thickness will affect the heat transfer characteristics. In this study, Pak and Cho's [26] equation has been used:

$$\mu_{nf} = \mu_{bf} \frac{(t_{nf}\rho_{nf})}{(t_{bf}\rho_{bf})} \quad (10)$$

$\mu_{nf}$ ,  $\mu_{bf}$  means the viscosity of the nanofluid and base fluid,  $t_{nf}$ , and  $t_{bf}$  refers to the nanofluid and base fluid temperature.

After calculating the values of the thermophysical properties of each nanofluid, the next step is to evaluate, analyze and realize the values with the values in the literature review to double-check our work before entering the simulation steps, Table 1 shows the density, and specific heat, thermal conductivity for the nanoparticles and viscosity for the liquids [27].

**Table 1**

The density, specific heat, thermal conductivity, and viscosity of liquids and nanoparticles

Materials	Density, $\rho$	Specific heat, Cp	Thermal conductivity, k	Viscosity, $\mu$
Water	998.2	4182	0.606	0.001003
Ethylene glycol	1116.6	2382	0.249	0.0161
Fe <sub>2</sub> O <sub>3</sub>	5240	628	12.552	
SnO <sub>2</sub>	6850	52.6	98	

#### 4. Grid Independent Test (GIT)

In general, the accuracy of the numerical results depends on the grid resolution. To estimate the number of the required elements of the current study five different element size has been investigated Figure 2 found 62878, 77354, and 122000 giving the same results that the 62878 elements number has been chosen. The pressure has not been changed and the mesh quality was 94.84%. The investigation has been made in a flat microchannel with water at 600 Re.

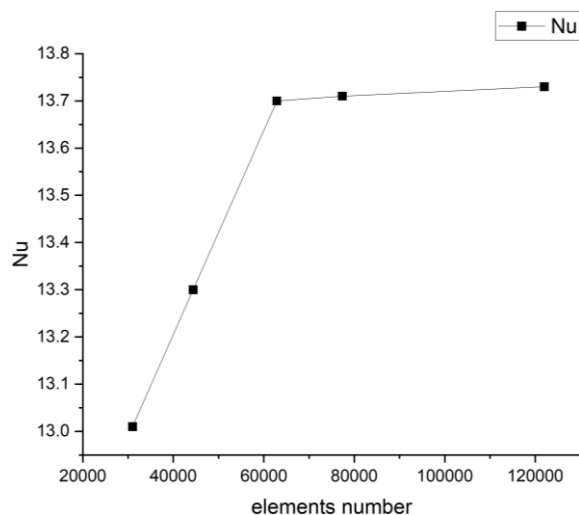


**Fig. 2.** The change in Nusselt number in different elements' number

#### 5. Validation of the Numerical Simulations

The numerical results are compared with the experimental and numerical studies from Wen and Ding [28] and Göktepe *et al.*, [29] in Figure 3. These researchers studied the heat transfer of laminar flow at 1050 Reynolds number in the flat microchannel.

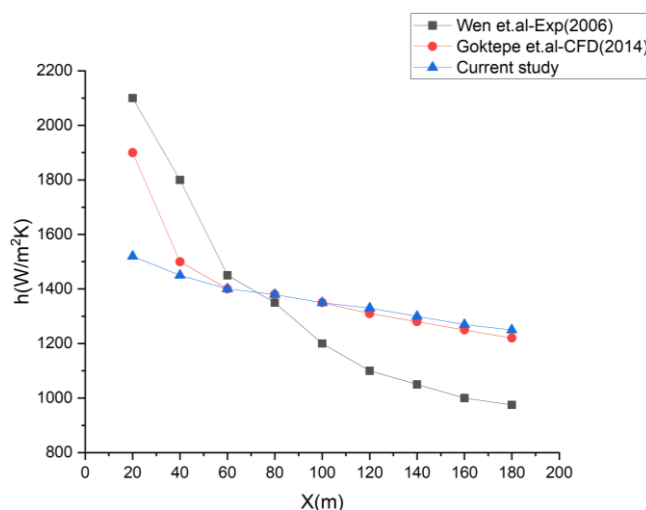


**Fig. 3.** Validation of present numerical results with numerical and experimental results of Wen and Ding [28] and Göktepe *et al.*, [29]

The numerical results of the Face step microchannel are compared with the experimental results from Abu Talib and Salman [30] and numerical results from Salman *et al.*, [31]. These authors studied the Nusselt number of turbulent flows of water. In Figure 4, comparison for the numerical results at Reynolds number of 5000 is shown, indicating that the results consist of the reference data. The accuracy of the numerical method is acceptable and the maximum error is less than 15%.

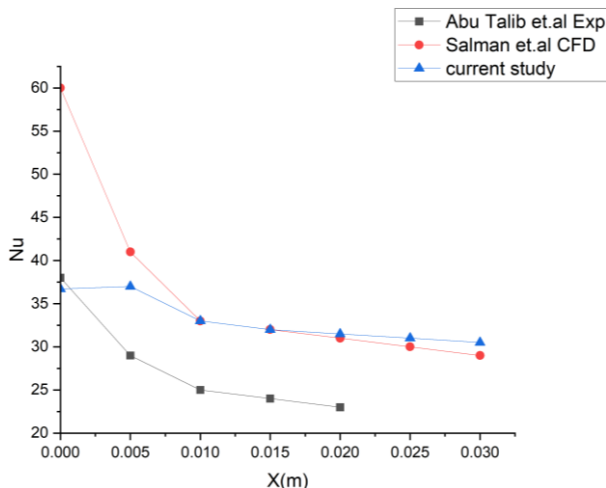


**Fig. 4.** The Nusselt number change (Abu Talib *et al.*, [30]) (Salman *et al.*, [31]) along the channel with water

Figure 5 presents the validation of the ethylene glycol at the face step microchannel at 5000 Reynolds number from (Salman *et al.*, [31]) numerical study at the same conditions. Hence, these results prove the validity of the CFD results with previous experimental and numerical studies.

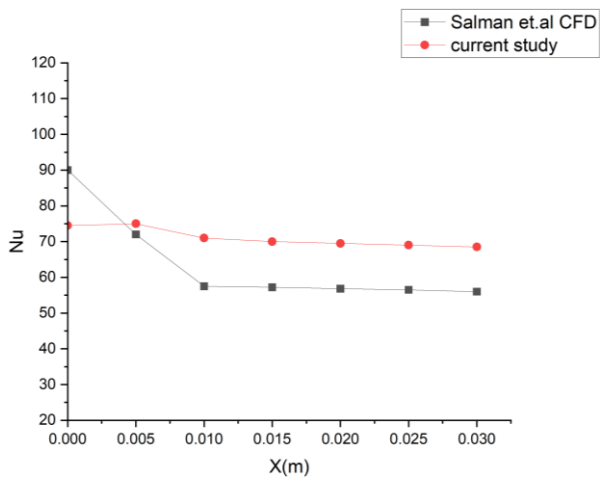


**Fig. 5.** The Nusselt number change from (Salman *et al.*, [31]) along the channel with ethylene glycol as fluid

## 6. Results and Discussions

### 6.1 The Effects of Microchannels in the Turbulent Flow with Ethylene Glycol as Base Fluid

This research presents and analyzes numerically the heat transfer performance of ethylene glycol as a base fluid. Current research studied the effect of the flat, face step, and radial microchannels

with different Reynolds numbers 4000-7000 Re with  $250 \text{ W/m}^2$  heat flux as shown in Figure 6. The wall temperature has been set at 300K. This section will study the average Nusselt number, pressure drop, and PEC of the different microchannels.

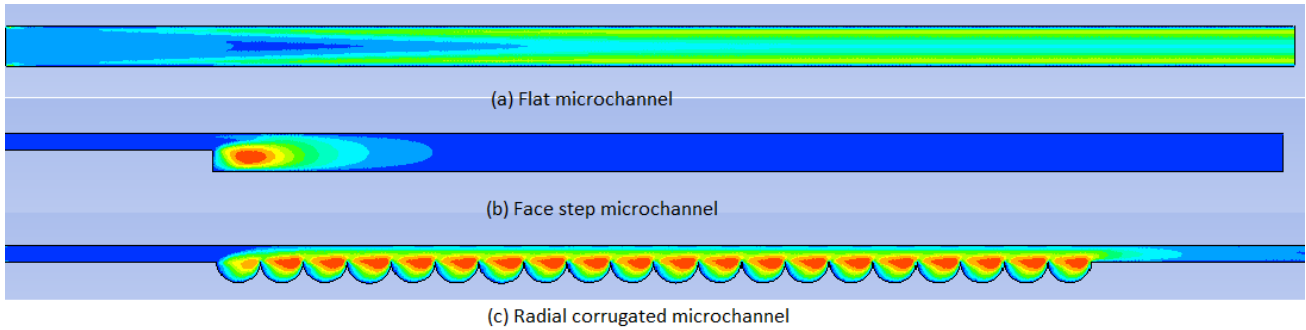


**Fig. 6.** Turbulent kinetic energy for the flat, face step and radial corrugated microchannel

**6.1.1 Effect of the microchannels on the average Nusselt number**

This section studies the effect of the different three microchannels on the average Nusselt number in different Reynolds numbers 4000-7000Re fluid flow. Figure 7 shows the Nu of the flat, face step, and Radial microchannels, the amount of the Nu increasing with the increase of the Reynolds number as expected and validated with the results in the previous studies.

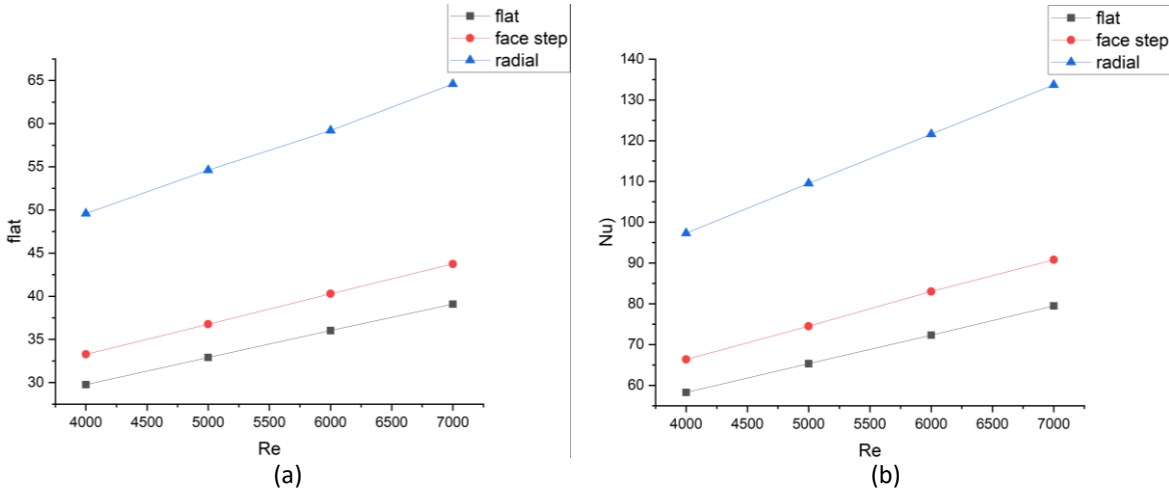


**Fig. 7.** (a) Reynolds number results of water, (b) Reynolds number results of ethylene glycol

By comparing the results found that the Nu increased in the face step microchannel compared to the flat in the water and ethylene glycol by 12% and 15% respectively with different Reynolds numbers 4000-7000Re.

The results show that the Nu increased in the Radial microchannel compared with flat in the water and ethylene glycol by 67% and 53% respectively. That increase happened due to the high turbulent circulation in radial corrugate and in the face step by a sudden increase in channel height and the increase of the surface area which led to the increase in the heat transfer performance of the channels.

### 6.1.2 Effect of microchannels on the pressure drop

This study part investigates the change in the pressure drop on flat, face step, and radial microchannels in 4000-7000 Re. Figure 8 shows the results that the radial corrugated microchannel has the highest pressure drop in turbulent flow conditions. This is because the pressure drops in the radial corrugated microchannel is more pronounced compared with the flat and face step channels and due to the large variance in the inlet and outlet channel pressure. As expected and presented in the previous studies that the flat microchannel got the lowest pressure drop, which is due to the absence of reverse turbulent fluid flow.

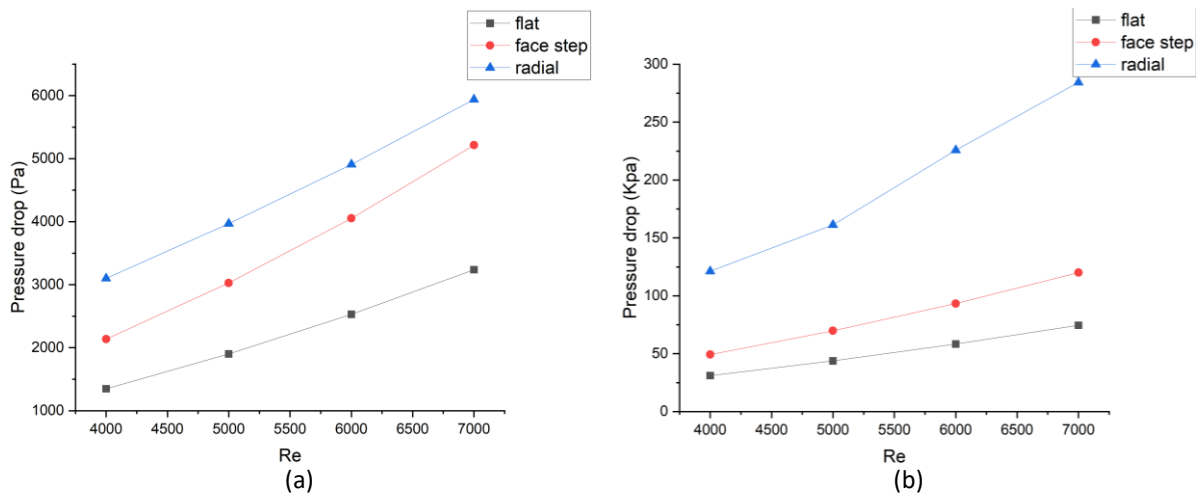


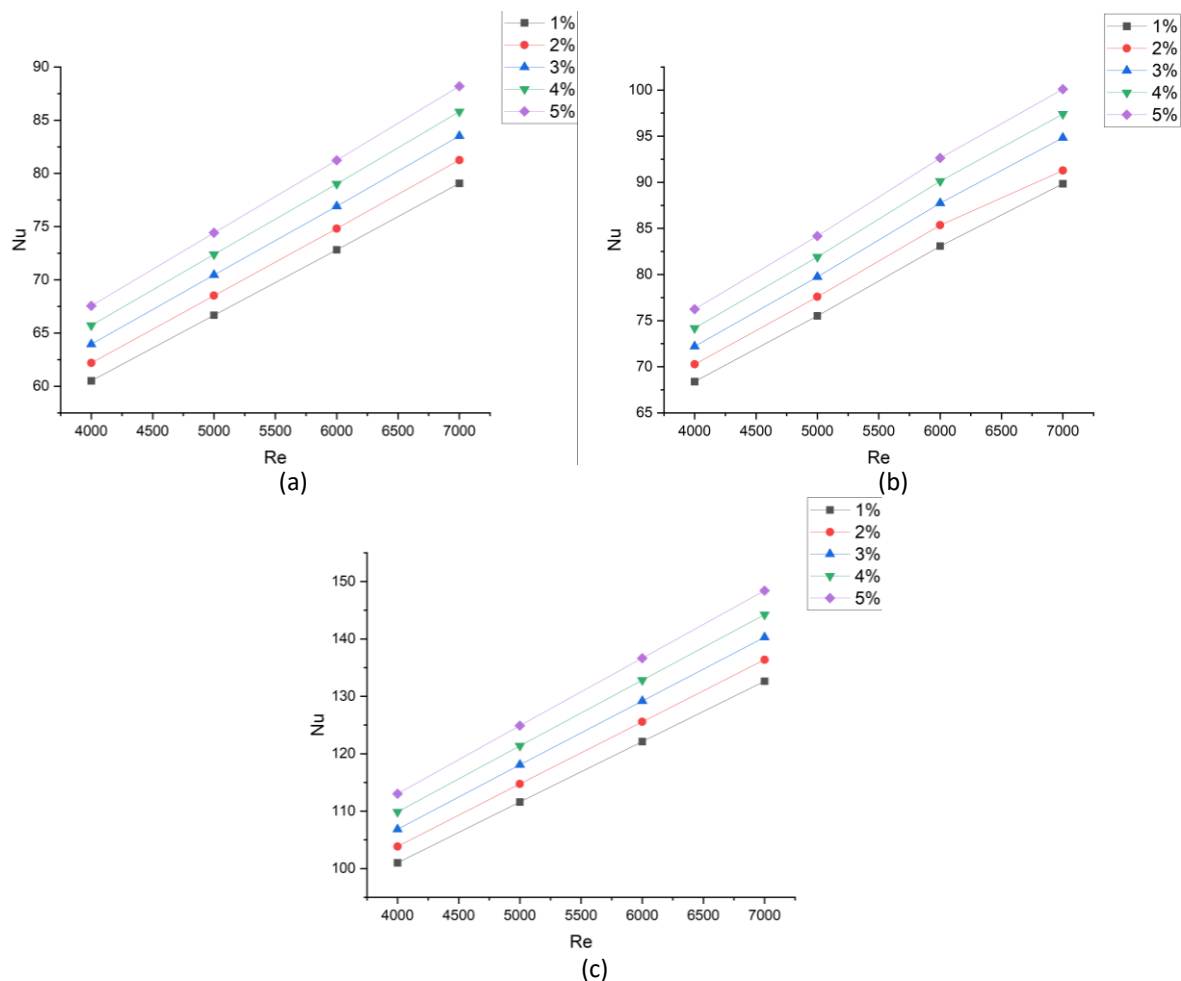
Fig. 8. (a) Pressure drop results of water, (b) pressure drop results of ethylene glycol

### 6.2 Study the Effect of $Fe_2O_3$ Nanofluid

This study presents the impact of the addition of  $Fe_2O_3$  ferric oxide in ethylene glycol as base fluid on the heat transfer and flow characteristics in the three different microchannels, the  $Fe_2O_3$  nanoparticles were with 1, 2, 3, 4 and 5% of concentrations, the results were calculated with a range of 4000-7000Re turbulent fluid flow.

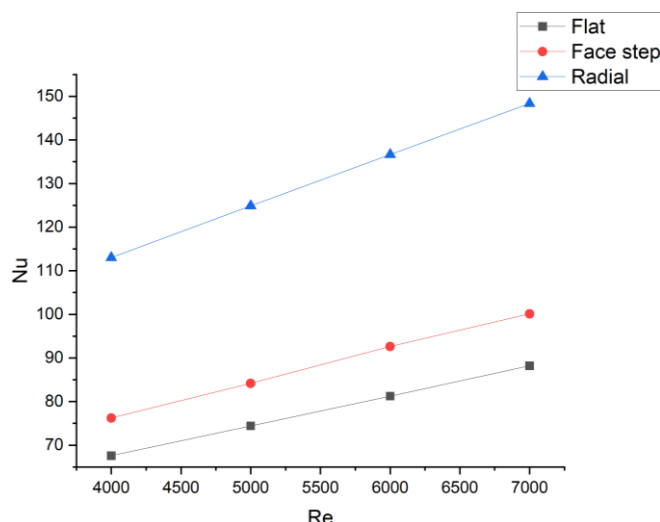
#### 6.2.1 Effect of $Fe_2O_3$ nanofluid on the Nusselt number

This part of the research investigates the enhancement that the  $Fe_2O_3$  nanoparticles can add to the ethylene glycol base fluid on the Nusselt number for the face step and radial comparing the results with the flat microchannels. Figure 9 presents the results of the investigation with a 4000-7000Re range and in 1, 2, 3, 4 and 5% of  $Fe_2O_3$  nanoparticles concentration.



**Fig. 9.** (a) Nusselt number values of Ferric oxide at the flat microchannel, (b) Nusselt number values of ferric oxide at Face step microchannel, (c) Nusselt number values of ferric oxide at the radial corrugated microchannel

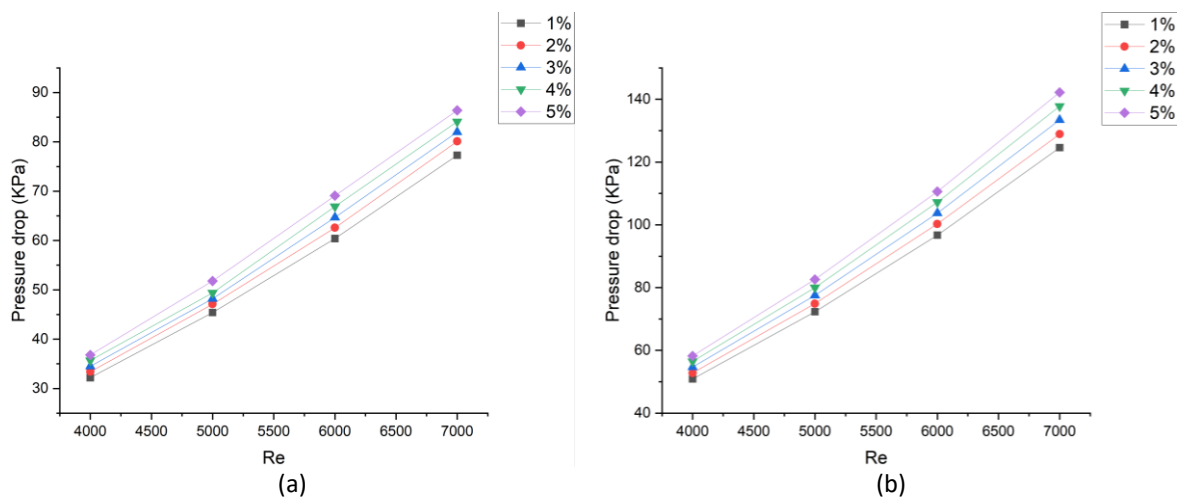
The results as presented in Figure 10 show that the Nusselt number increase with the increase of the  $Fe_2O_3$  nanoparticles concentration in the ethylene glycol base fluid in all microchannels. The flat microchannels Nusselt number increased by 11% at 7000Re with 5% of volume concentration by 11% and 10% in the face step and 11% in the radial corrugated microchannel. The radial microchannel got the highest Nusselt number compared with flat and face step channels because of the increase in the wall surface area. The results found that by comparing the radial corrugated microchannel with  $Fe_2O_3$  nanofluid 5% of concentration at 4000-7000Re with ethylene glycol base fluid in flat microchannel the increase was 94-87% and with the face step microchannel was from 70 to 63%.



**Fig. 10.** Nusselt number values of 5% of ferric oxide at different microchannels

### 6.2.2 Effect of $Fe_2O_3$ nanofluid on the pressure drop

The effect of Reynolds number and nanoparticles concentrations on pressure drop are presented in Figure 11 and Figure 12. The results show that the pressure drop increased with the increase of Reynolds number and with the increase in the concentration of the nanoparticles and these results validated with the previous studies that explain the increase in the fluid viscosity and density leading to increase the pressure drop.



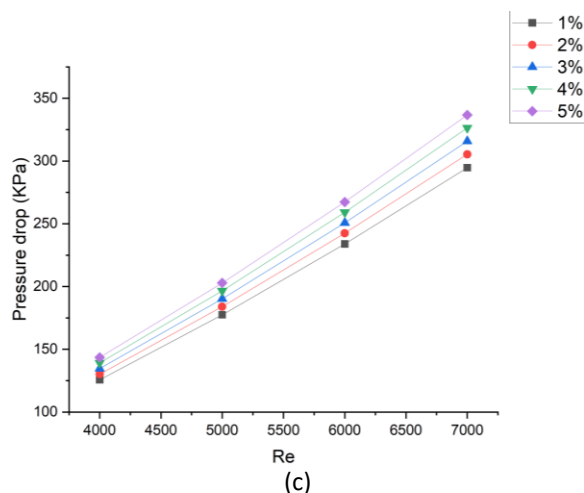


**Fig. 11.** (a) Pressure drop results of ferric oxide in the flat microchannel, (b) pressure drop results of ferric oxide in face step microchannel, (c) pressure drop results of ferric oxide in radial corrugated microchannel

Pressure drops results mean the difference of the pressure between the inlet and outlet of the channel domain, these results present whether the change of the channel shape and the increase in the volume concentration (1, 2, 3, 4 and 5%) and Reynolds number (4000-7000Re), the results of the show that the pressure drop increase with the increase of the Reynolds number and nanoparticles concentrations. Figure 12 presents the flat microchannel pressure drop change, pressure drop increased from 4000 Re to 7000 Re by 140% times at 5% of volume concentration and comparing the results of ethylene glycol base fluid with 5% of ferric oxide at 7000 Re increased 18.7%. Another hand, comparing the same conditions with a flat microchannel increased with Reynolds number up to 144% from 4000 Re to 7000Re and from Ethylene glycol with 5% of ferric oxide up to 18.5%. lastly with the Radial corrugated microchannel, at different Reynolds numbers, the increment was 134.5% and 14.1% between ethylene glycol and 5% ferric oxide.

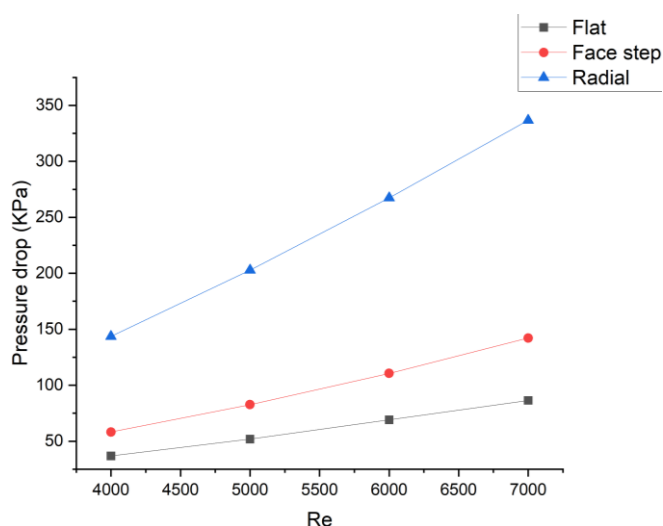


**Fig. 12.** Pressure drop results of 5% ferric oxide in different microchannels

The upper plot presents the difference in pressure drop for the three microchannels (Flat, face step, Radial) with 4000 Re to 7000 Re at 5% of ferric oxide suspended in ethylene glycol as base fluid. The Radial microchannel scored the highest pressure drop compared with other channels at all four

Reynolds number gradients. At 7000 Re the gap increased for the Radial corrugated microchannel up to 3.9 times more than the flat microchannel.

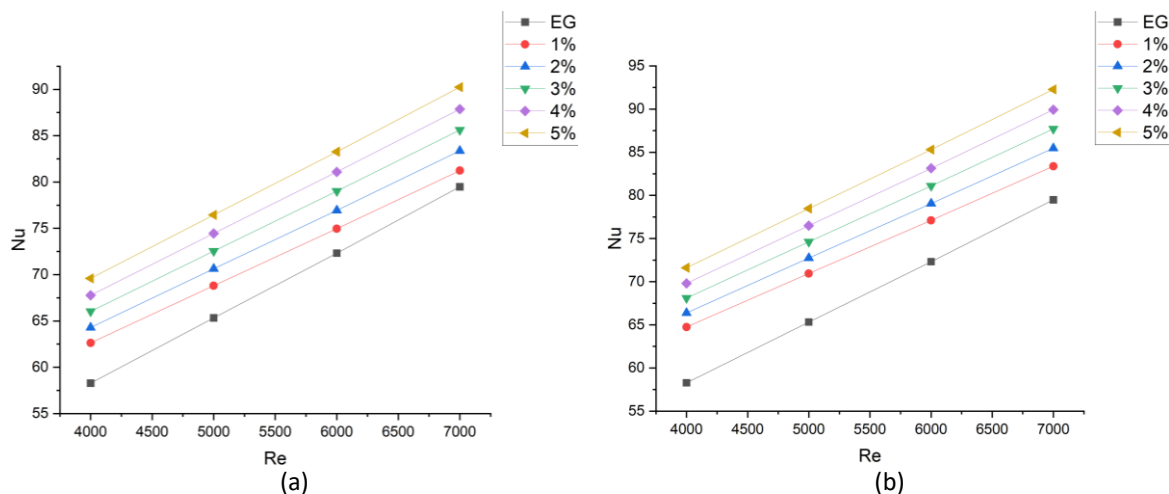
### 6.3 Effect of using Hybrid Nanofluid

This part of the study investigates numerically the thermal properties of the hybrid nanofluid the concentrations of SnO<sub>2</sub> was 5% to 95% of Fe<sub>2</sub>O<sub>3</sub> and 15% SnO<sub>2</sub> to 85% of Fe<sub>2</sub>O<sub>3</sub> in the calculations. The base fluid was ethylene glycol and the volume concentrations of the nanoparticles that have been suspended in the ethylene glycol (1, 2, 3, 4 and 5%). The study was in turbulent fluid flow with 4000-7000Re Reynolds number range in flat, face step, and radial corrugated microchannels.

#### 6.3.1 Effect of using hybrid nanofluid on the Nusselt number

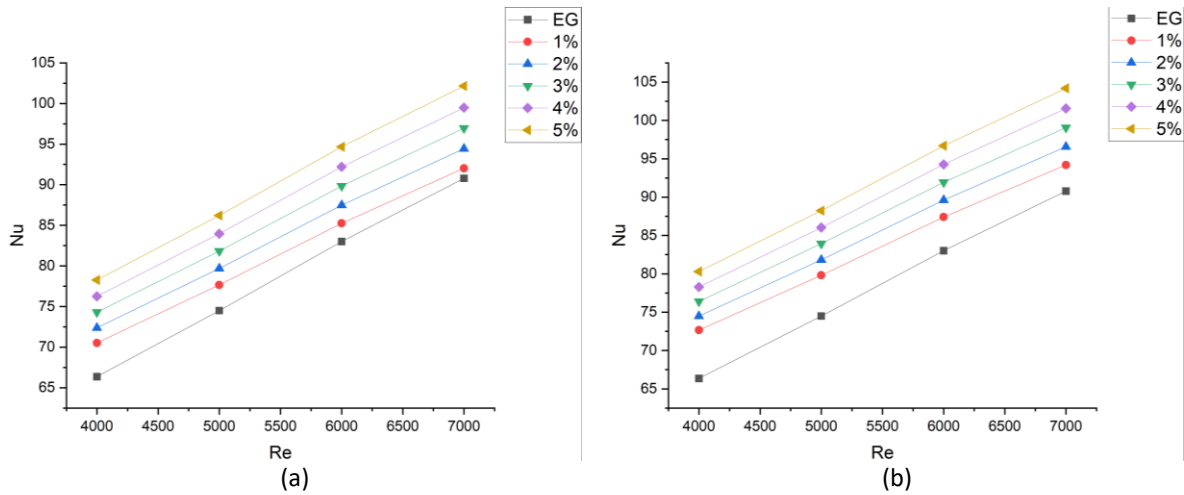
The results of this investigation have been evaluated in Figure 13 to Figure 15, which show the increase in the Nusselt number with the increase of the volume concentration from 1 to 5% of the nanoparticles in both SnO<sub>2</sub> 5%-Fe<sub>2</sub>O<sub>3</sub> 95% and SnO<sub>2</sub> 15%-Fe<sub>2</sub>O<sub>3</sub> 85%. The increase has been noticed in the three microchannels.

Figure 13 presents the Nusselt number calculations of the hybrid nanofluid in a flat microchannel with 1, 2, 3, 4 and 5 volume concentrations and with a range of 4000-7000 Re Reynolds number of turbulent fluid flow, the results have been compared with the ethylene glycol which has been used as the base fluid, the plots show that the Nusselt number increasing with the increase of the Reynolds number and with an increase of the hybrid concentration. The hybrid Nusselt number increased highest at 5% of hybrid volume concentration and 7000 Re by 13.5% at 5% of Tin oxide and 16%.



**Fig. 13.** (a) Nusselt number results of 5% (SFO) in the flat microchannel, (b) Nusselt number results of 15% (SFO) in flat microchannel

Face step microchannel has been studied numerically in Figure 14 to evaluate its thermal performance with the addition of the SnFe<sub>2</sub>O<sub>3</sub> hybrid nanofluid. The results show an enhancement with the increase of the Reynolds number and hybrid nanoparticles concentration, the Nusselt number got the highest increase at 5% of hybrid nanofluid at 7000 Re compared with the base fluid increased by 12.5% and 14.8% in 5% and 15% of the tin oxide- ferric oxide hybrid nanofluid.



**Fig. 14.** (a) Nusselt number results of 5% (SFO) in face step microchannel, (b) Nusselt number results of 15% (SFO) in face step microchannel

In Figure 15, the Nusselt number has been investigated for hybrid nanofluids in the Radial corrugated microchannel, the results show that the increase of volume concentration and Reynolds number leads to an increase in the Nusselt number, the incensement of the Nusselt number at 5Sn95Fe2O3 of Hybrid nanofluid was 13.3% and 15.6% at 15Sn85Fe2O3. In figure 16 present the change in the Nusselt number amount in the wall of the flat, face step and radial microchannel. The conclusion of this part is shown in Figure 17. As it is seen, the radial corrugated microchannel got the highest amount of Nusselt number, and the enhancement of the 15% of tin oxide with 85% of ferric oxide hybrid nanofluid in the radial microchannel compared with the ethylene glycol in the flat microchannel was 94.4% at 7000 Re.

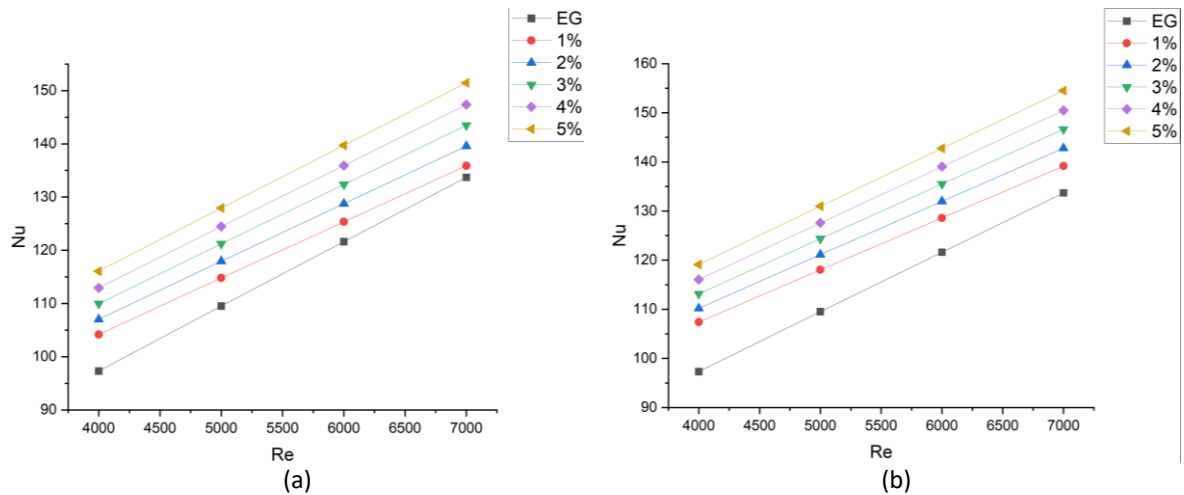


**Fig. 15.** (a) Nusselt number results of 5% (SFO) in the radial corrugated microchannel, (b) Nusselt number results of 15% (SFO) in radial corrugated microchannel

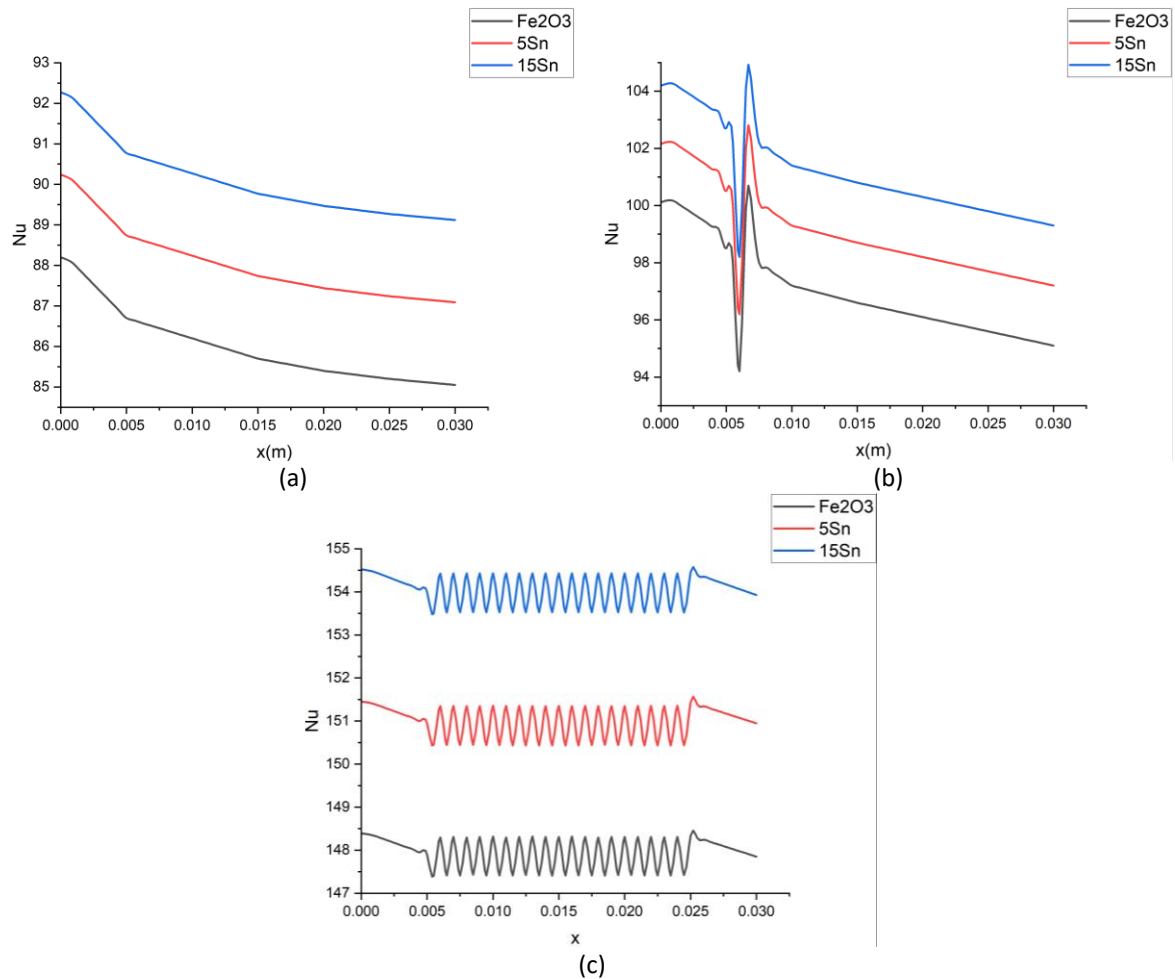


**Fig. 16.** (a) Nusselt number results in the flat microchannel at 5% of volume concentration for the nanofluids, (b) Nusselt number results in face step microchannel at 5% of volume concentration for the nanofluids, (c) Nusselt number results in the radial corrugated microchannel at 5% of volume concentration for the nanofluids

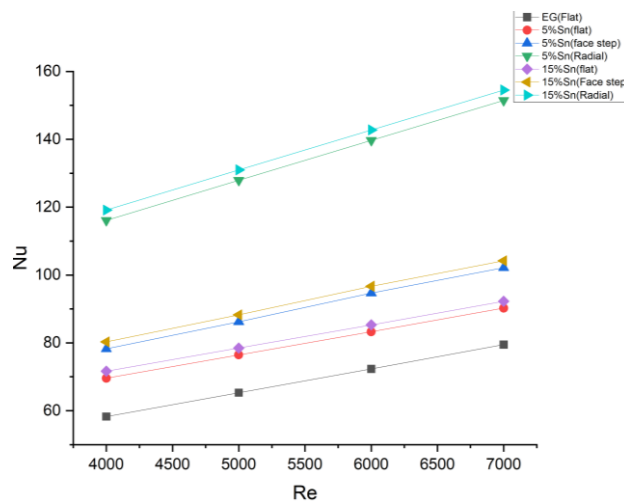


**Fig. 17.** Nusselt number comparative for the 5% volume concentration at different nanofluids in the three microchannels

### 6.3.2 Effect of using hybrid nanofluid on the pressure drop

The pressure drop has been calculated numerically using the CFD (ANSYS) program by calculating the inlet and outlet pressure of the channel, this part focusing on the effect of the Tin oxide with ferric oxide as 5% and 15% hybrid nanofluid with ethylene glycol as base fluid, the results have been confirmed with the conclusion in the pressure drop calculations in the previous studies, that the pressure drop increase with the increase in the volume concentrations and with the increase in the Reynolds number.

As shown in Figure 18 which are the plots of the hybrid nanofluids in the flat microchannel, it can tell that the pressure drop increased with the increase of Reynolds number, the change of the hybrid volume concentration led to an increase in the pressure drop by 19% at 5% of  $^{55}\text{Sn}^{95}\text{Fe}_2\text{O}_3$  and 19.7% compared with ethylene glycol.

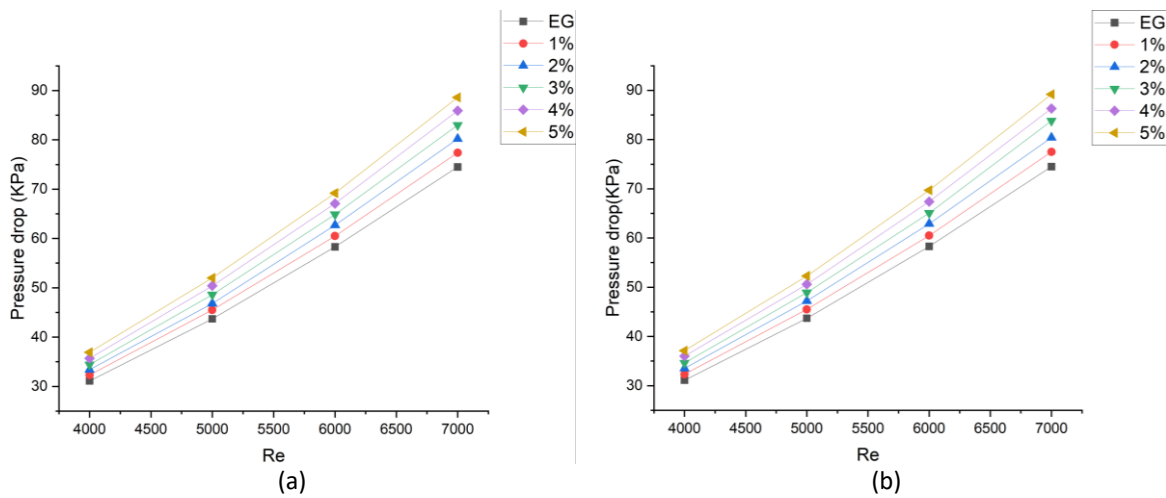


**Fig. 18.** (a) Pressure drop results of 5% (SFO) in the flat microchannel, (b) pressure drop results of 15% (SFO) in the flat microchannel

The face step microchannel pressure drop has been increased with the increase of the Reynolds number and with the increasing of SnO<sub>2</sub> doping increase as presented in figure 19 same as with the increase of nanofluid concentration

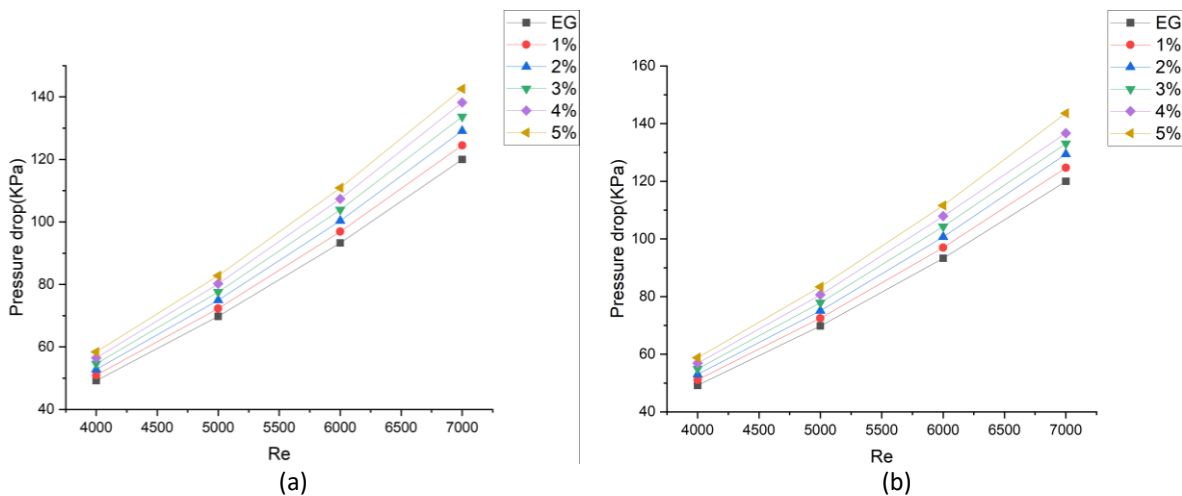


**Fig. 19.** (a) Pressure drop results of 5% (SFO) in face step microchannel, (b) pressure drop results of 15% (SFO) in face step microchannel

In the radial corrugated microchannel as shown in Figure 20, the pressure drop has increased with the increase of the hybrid nanoparticles concentration up to 18.8% at 5Sn hybrid nanofluid and up to 19.5% at the  $^{15}\text{Sn}^{85}\text{Fe}_2\text{O}_3$ .

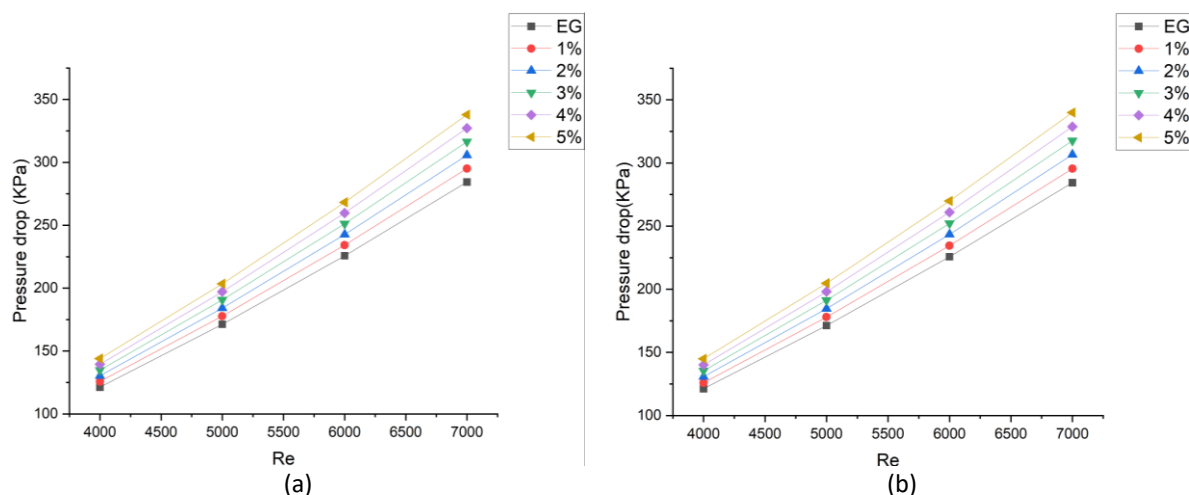


**Fig. 20.** (a) Pressure drop results of 5% (SFO) in the radial corrugated microchannel, (b) pressure drop results of 15% (SFO) in radial corrugated microchannel

From the plot of the pressure drop investigation in Figure 21, we can notice that the incensement between the microchannels is higher than the increase between the hybrid nanofluids compared with ethylene glycol the base fluid, the highest value as at 5% of volume concentration of  $^{15}\text{Sn}^{85}\text{Fe}_2\text{O}_3$  comparing with the ethylene glycol in flat microchannel up to 4.5 times.

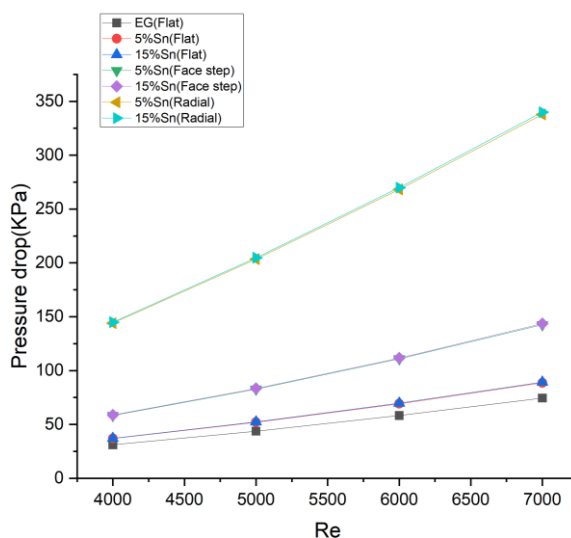


**Fig. 21.** Pressure drop results comparative for the 5% volume concentration at different nanofluids and the three microchannels

#### 6.4 Performance Evaluation Criteria (PEC)

The previous sections studied numerically the flow and heat transfer behavior of the  $\text{Fe}_2\text{O}_3$  nanofluid with ethylene glycol as base fluid and the addition of the tin oxide as 5% and 15% to the ferric oxide at 5 different gradients of volume concentrations (1, 2, 3, 4 and 5%) with flat, face step and Radial corrugated microchannels, the PEC criteria method has been studied widely and it has

been significantly approved by many researchers in this field. PEC has been defined in the following [32]:

$$PEC = \frac{(Nu_{nf}/Nu_{EG,flat})}{(f_{nf}/f_{EG,flat})^{1/3}} \quad (11)$$

$Nu_{nf}$  means nanofluid Nusselt number,  $Nu_{EG,flat}$  means the Nusselt number of ethylene glycol in the flat microchannel,  $f_{nf}$  refers to the skin friction factor of nanofluid,  $f_{EG,flat}$  means skin friction factor of ethylene glycol in the flat microchannel.

PEC criteria can tell if the conditions of the study got an advantage compared with the base condition which is the flat microchannel with ethylene glycol if the PEC value was equal to 1 or less means no advantage has been found, if the PEC value is more than 1 means the thermal performance is higher than the base case study.

Figure 22 presents the PEC plot of the flat microchannel with the ferric oxide and with the hybrid Tin oxide in ferric oxide in 5% and 15% concentration percentages suspended in ethylene glycol as base fluid, the numerical calculations found that the PEC decreased with the increase of Reynolds number in all cases, and found that the PEC increase with the increase of the nanoparticles volume concentration, the PEC in  $^{15}\text{Sn}^{85}\text{Fe}_2\text{O}_3$  at 5% of concentration at 4000 Re got the highest enhancement about 22.9% increase compared with ethylene glycol at same conditions followed by the hybrid  $^{5}\text{Sn}^{85}\text{Fe}_2\text{O}_3$  by 19.4%.

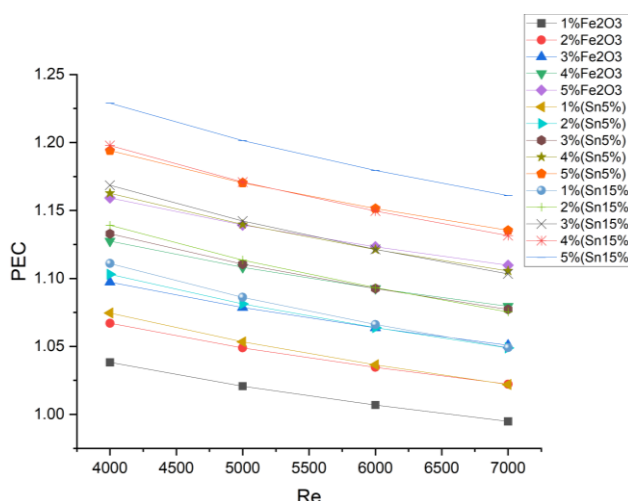
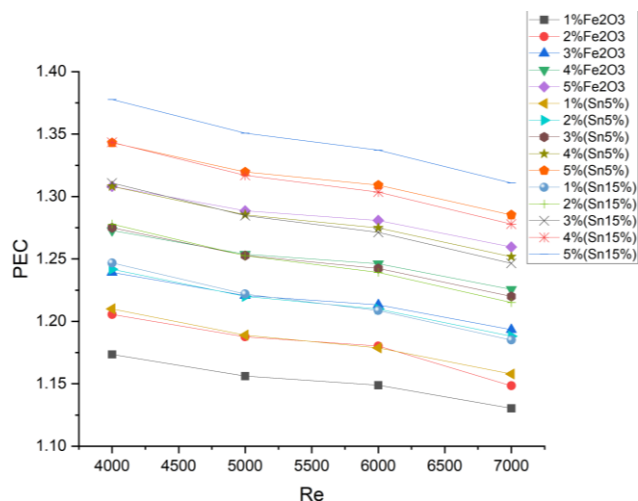


Fig. 22. PEC results for the flat microchannel

PEC investigation of the face step microchannel has been presented in Figure 23. The results showed that the thermal performance criteria decreased with the increase of Reynolds number and increases with the increase in nanofluid volume concentration, the calculations showed that the PEC investigation got the highest value in 5% of  $^{15}\text{Sn}^{85}\text{Fe}_2\text{O}_3$  by 37.8% and 34.3% for the  $^{5}\text{Sn}^{95}\text{Fe}_2\text{O}_3$  hybrid nanofluid.



**Fig. 23.** PEC results for the face step microchannel

The PEC evaluation for the Radial corrugated microchannel is presented in Figure 24 got the highest value compared with the flat and face step microchannels, the thermal performance has been increased by 104.3% with the <sup>15</sup>Sn<sup>85</sup>Fe<sub>2</sub>O<sub>3</sub> of 5% of volume concentration compared with the ethylene glycol in the flat microchannel.

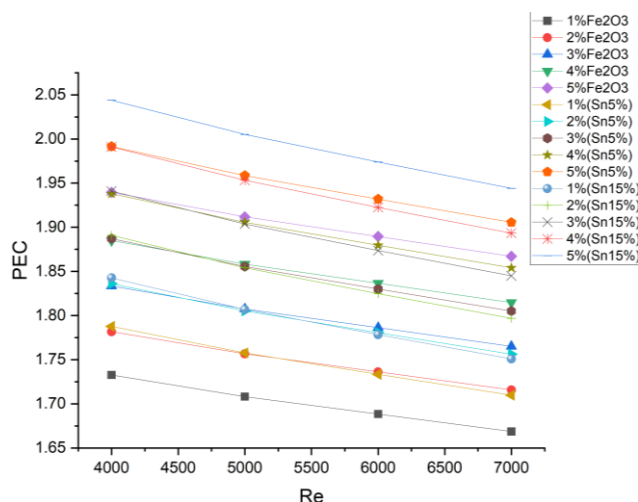


**Fig. 24.** PEC results for the radial corrugated microchannel

The performance evaluation criteria value has increased by 82% from flat microchannel to radial microchannel at 5% of volume concentration of <sup>15</sup>Sn<sup>85</sup>Fe<sub>2</sub>O<sub>3</sub> hybrid nanofluid as shown in Figure 25.

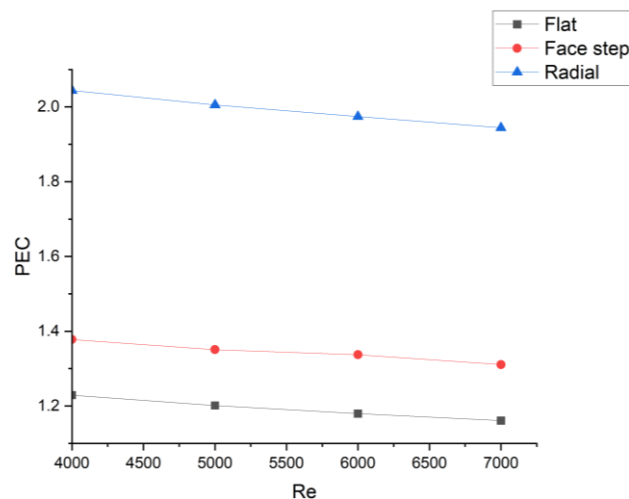


**Fig. 25.** PEC results of  $^{15}\text{Sn}^{85}\text{Fe}_2\text{O}_3$  at 5% volume concentration for the three microchannel

## 7. Conclusion

The numerical investigation has been made of 2-D turbulent mixed convection fluid flow in flat, face step and radial corrugated microchannels, this study has studied the hybrid ferric oxide with tin oxide at (0, 5, 15%) with ethylene glycol as base fluid, with (1, 2, 3, 4, 5 %) of volume concentrations at Reynolds number range with (4000-7000) Re. The outcomes reveal that the Nusselt number and pressure drop values increased with the increase of volume concentration and Reynolds number.

The results showed that Nusselt number results in ethylene glycol got higher than in water as well as in pressure drop.

The Radial corrugated microchannel got the highest Nusselt number, pressure drop, and skin friction coefficient followed by the face step and then flat microchannels.  $^{15}\text{Sn}^{85}\text{Fe}_2\text{O}_3$  hybrid nanofluid suspended in ethylene glycol at 5% volume concentration got the highest Nusselt number, pressure drop, and skin friction coefficient followed by  $^{5}\text{Sn}^{95}\text{Fe}_2\text{O}_3$  hybrid nanofluid then the ferric oxide  $\text{Fe}_2\text{O}_3$ .

Performance evaluation criteria (PEC) studied the heat transfer in all study steps and found that the  $^{15}\text{Sn}^{85}\text{Fe}_2\text{O}_3$  hybrid nanofluid in ethylene glycol at 5% volume concentration in radial corrugated microchannel increased 104% compared with ethylene glycol in the flat microchannel. The performance evaluation criteria value has increased by 82% from Flat microchannel to Radial microchannel at 5% of volume concentration of  $^{15}\text{Sn}^{85}\text{Fe}_2\text{O}_3$  hybrid nanofluid.

## Acknowledgment

This research was not funded by any grant.

## References

- [1] Akbari, Omid Ali, Davood Toghraie, and Arash Karimipour. "Impact of ribs on flow parameters and laminar heat transfer of water-aluminum oxide nanofluid with different nanoparticle volume fractions in a three-dimensional rectangular microchannel." *Advances in Mechanical Engineering* 7, no. 11 (2015): 1687814015618155. <https://doi.org/10.1177/1687814015618155>
- [2] Dogonchi, A. S., Ali J. Chamkha, S. M. Seyyedi, and D. D. Ganji. "Radiative nanofluid flow and heat transfer between parallel disks with penetrable and stretchable walls considering Cattaneo-Christov heat flux model." *Heat Transfer-Asian Research* 47, no. 5 (2018): 735-753. <https://doi.org/10.1002/htj.21339>

- [3] Thumma, Thirupathi, O. Anwar Bég, and A. Kadir. "Numerical study of heat source/sink effects on dissipative magnetic nanofluid flow from a non-linear inclined stretching/shrinking sheet." *Journal of Molecular Liquids* 232 (2017): 159-173. <https://doi.org/10.1016/j.molliq.2017.02.032>
- [4] Eshgarf, Hamed, Afshin Ahmadi Nadooshan, and Afrasiab Raisi. "A review of multi-phase and single-phase models in the numerical simulation of nanofluid flow in heat exchangers." *Engineering Analysis with Boundary Elements* 146 (2023): 910-927. <https://doi.org/10.1016/j.enganabound.2022.10.013>
- [5] Alklaibi, A. M., Kotturu V. V. Chandra Mouli, and L. Syam Sundar. "Experimental investigation of heat transfer and effectiveness of employing water and ethylene glycol mixture based Fe<sub>3</sub>O<sub>4</sub> nanofluid in a shell and helical coil heat exchanger." *Thermal Science and Engineering Progress* 40 (2023): 101739. <https://doi.org/10.1016/j.tsep.2023.101739>
- [6] Chiam, H. W., W. H. Azmi, N. M. Adam, and M. K. A. M. Ariffin. "Numerical study of nanofluid heat transfer for different tube geometries-A comprehensive review on performance." *International Communications in Heat and Mass Transfer* 86 (2017): 60-70. <https://doi.org/10.1016/j.icheatmasstransfer.2017.05.019>
- [7] Shah, Zahir, Poom Kumam, and Wejdan Deebani. "Radiative MHD Casson Nanofluid Flow with Activation energy and chemical reaction over past nonlinearly stretching surface through Entropy generation." *Scientific Reports* 10, no. 1 (2020): 4402. <https://doi.org/10.1038/s41598-020-61125-9>
- [8] Choi, S. US, and Jeffrey A. Eastman. *Enhancing thermal conductivity of fluids with nanoparticles*. No. ANL/MSD/CP-84938; CONF-951135-29. Argonne National Lab.(ANL), Argonne, IL (United States), 1995.
- [9] Wang, Xinwei, Xianfan Xu, and Stephen US Choi. "Thermal conductivity of nanoparticle-fluid mixture." *Journal of Thermophysics and Heat Transfer* 13, no. 4 (1999): 474-480. <https://doi.org/10.2514/2.6486>
- [10] Afshari, Faraz, Azim Doğuş Tuncer, Adnan Sözen, Halil Ibrahim Variyenli, Ataollah Khanlari, and Emine Yağız Gürbüz. "A comprehensive survey on utilization of hybrid nanofluid in plate heat exchanger with various number of plates." *International Journal of Numerical Methods for Heat & Fluid Flow* 32, no. 1 (2022): 241-264. <https://doi.org/10.1108/HFF-11-2020-0743>
- [11] Hassan, Qais Hussein, Shaalan Ghanam Afluo, and Mohamed Abed Al Abas Siba. "Numerical investigation of heat transfer in car radiation system using improved coolant." *Journal of Advanced Research in Fluid Mechanics and Thermal Sciences* 83, no. 1 (2021): 61-69. <https://doi.org/10.37934/arfm.83.1.6169>
- [12] Nashee, Sarah Rabee, and Haiyder Minin Hmood. "Numerical Study of Heat Transfer and Fluid Flow over Circular Cylinders in 2D Cross Flow." *Journal of Advanced Research in Applied Sciences and Engineering Technology* 30, no. 2 (2023): 216-224. <https://doi.org/10.37934/araset.30.2.216224>
- [13] Muhammad, Noor, and Sohail Nadeem. "Ferrite nanoparticles Ni-ZnFe<sub>2</sub>O<sub>4</sub>, Mn-ZnFe<sub>2</sub>O<sub>4</sub> and Fe<sub>2</sub>O<sub>4</sub> in the flow of ferromagnetic nanofluid." *The European Physical Journal Plus* 132 (2017): 1-12. <https://doi.org/10.1140/epjp/i2017-11650-2>
- [14] Kleinstreuer, Clement, and Yu Feng. "Experimental and theoretical studies of nanofluid thermal conductivity enhancement: a review." *Nanoscale Research Letters* 6 (2011): 1-13. <https://doi.org/10.1186/1556-276X-6-229>
- [15] Das, Sarit Kumar, Stephen U. S. Choi, and Hrishikesh E. Patel. "Heat transfer in nanofluids-a review." *Heat Transfer Engineering* 27, no. 10 (2006): 3-19. <https://doi.org/10.1080/01457630600904593>
- [16] Yu, Wenhua, David M. France, Jules L. Routbort, and Stephen U. S. Choi. "Review and comparison of nanofluid thermal conductivity and heat transfer enhancements." *Heat Transfer Engineering* 29, no. 5 (2008): 432-460. <https://doi.org/10.1080/01457630701850851>
- [17] Salman, S., A. R. Abu Talib, S. Saadon, and M. T. Hameed Sultan. "Hybrid nanofluid flow and heat transfer over backward and forward steps: A review." *Powder Technology* 363 (2020): 448-472. <https://doi.org/10.1016/j.powtec.2019.12.038>
- [18] Urmi, Wajiha Tasnim, A. S. Shafiqah, Md Mustafizur Rahman, Kumaran Kadirgama, and Md Abdul Maleque. "Preparation methods and challenges of hybrid nanofluids: a review." *Journal of Advanced Research in Fluid Mechanics and Thermal Sciences* 78, no. 2 (2020): 56-66. <https://doi.org/10.37934/arfm.78.2.5666>
- [19] Ajith, K., I. V. Muthuvijayan Enoch, A. Brusly Solomon, and Archana Sumohan Pillai. "Characterization of magnesium ferrite nanofluids for heat transfer applications." *Materials Today: Proceedings* 27 (2020): 107-110. <https://doi.org/10.1016/j.matpr.2019.09.014>
- [20] Bazdar, Hamed, Davood Toghraie, Farzad Pourfattah, Omid Ali Akbari, Hoang Minh Nguyen, and Amin Asadi. "Numerical investigation of turbulent flow and heat transfer of nanofluid inside a wavy microchannel with different wavelengths." *Journal of Thermal Analysis and Calorimetry* 139 (2020): 2365-2380. <https://doi.org/10.1007/s10973-019-08637-3>
- [21] Firlianda, Dinda Anggara, Avita Ayu Permanasari, Poppy Puspitasari, and Sukarni Sukarni. "Heat transfer enhancement using nanofluids (MnFe<sub>2</sub>O<sub>4</sub>-ethylene glycol) in mini heat exchanger shell and tube." In *AIP Conference Proceedings*, vol. 2120, no. 1. AIP Publishing, 2019. <https://doi.org/10.1063/1.5115690>

- [22] Moraveji, Mostafa Keshavarz, and Reza Mohammadi Ardehali. "CFD modeling (comparing single and two-phase approaches) on thermal performance of Al<sub>2</sub>O<sub>3</sub>/water nanofluid in mini-channel heat sink." *International Communications in Heat and Mass Transfer* 44 (2013): 157-164. <https://doi.org/10.1016/j.icheatmasstransfer.2013.02.012>
- [23] Manay, Eyuphan, and Bayram Sahin. "Heat transfer and pressure drop of nanofluids in a microchannel heat sink." *Heat Transfer Engineering* 38, no. 5 (2017): 510-522. <https://doi.org/10.1080/10407782.2016.1195162>
- [24] Ben-Mansour, R., and M. A. Habib. "Use of nanofluids for improved natural cooling of discretely heated cavities." *Advances in Mechanical Engineering* 5 (2013): 383267. <https://doi.org/10.1155/2013/383267>
- [25] Xuan, Yimin, and Wilfried Roetzel. "Conceptions for heat transfer correlation of nanofluids." *International Journal of Heat and Mass Transfer* 43, no. 19 (2000): 3701-3707. [https://doi.org/10.1016/S0017-9310\(99\)00369-5](https://doi.org/10.1016/S0017-9310(99)00369-5)
- [26] Pak, Bock Choon, and Young I. Cho. "Hydrodynamic and heat transfer study of dispersed fluids with submicron metallic oxide particles." *Experimental Heat Transfer an International Journal* 11, no. 2 (1998): 151-170. <https://doi.org/10.1080/08916159808946559>
- [27] Lide, David R., ed. *CRC handbook of chemistry and physics*. Vol. 85. CRC Press, 2004.
- [28] Wen, Dongsheng, and Yulong Ding. "Experimental investigation into convective heat transfer of nanofluids at the entrance region under laminar flow conditions." *International Journal of Heat and Mass Transfer* 47, no. 24 (2004): 5181-5188. <https://doi.org/10.1016/j.ijheatmasstransfer.2004.07.012>
- [29] Göktepe, Sinan, Kunt Atalık, and Hakan Ertürk. "Comparison of single and two-phase models for nanofluid convection at the entrance of a uniformly heated tube." *International Journal of Thermal Sciences* 80 (2014): 83-92. <https://doi.org/10.1016/j.ijthermalsci.2014.01.014>
- [30] Abu Talib, Abd Rahim, and Sadeq Salman. "Heat transfer and fluid flow analysis over the microscale backward-facing step using  $\beta$ Ga<sub>2</sub>O<sub>3</sub> nanoparticles." *Experimental Heat Transfer* 36, no. 3 (2023): 358-375. <https://doi.org/10.1080/08916152.2022.2039328>
- [31] Salman, Sadeq, Abd Rahim Abu Talib, Ali Hilo, Sadeq Rashid Nfawa, Mohamed Thariq Hameed Sultan, and Syamimi Saadon. "Numerical study on the turbulent mixed convective heat transfer over 2d microscale backward-facing step." *CFD Letters* 11, no. 10 (2019): 31-45.
- [32] Manca, Oronzio, Sergio Nardini, and Daniele Ricci. "A numerical study of nanofluid forced convection in ribbed channels." *Applied Thermal Engineering* 37 (2012): 280-292. <https://doi.org/10.1016/j.applthermaleng.2011.11.030>